Table of Contents (TOC)

Aggregation-Induced Emission

Andong Shao, Yongshu Xie, Shaojia Zhu, Zhiqian Guo, Shiqin Zhu, Jin Guo, Ping Shi, Tony D. James, He Tian, and Wei-Hong Zhu** ____ ***Page – Page***

Far-Red and Near-Infrared AIE-Active Fluorescent Organic Nanoprobes with Enhanced Tumor-Targeting Efficacy: Shape-Specific Effects

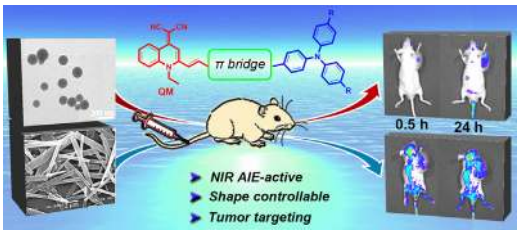

Tailoring long wavelength aggregation-induced emission (AIE)-active molecules affords organic nanoaggregates with desired morphology from rod-like to spherical, highly preferable for enhanced tumor-targeted bioimaging *in vivo*.

Far-Red and Near-Infrared AIE-Active Fluorescent Organic Nanoprobes with Enhanced Tumor-Targeting Efficacy: Shape-Specific Effects

Andong Shao, Yongshu Xie, Shaojia Zhu, Zhiqian Guo, Shiqin Zhu, Jin Guo, Ping Shi, Tony D. James, He Tian, and Wei-Hong Zhu**

---

[*] A. Shao,[+] Prof. Dr. Y. Xie,[+] S. Zhu, Dr. Z. Guo, S. Zhu, Prof. Dr. P. Shi, Prof. Dr. H. Tian, Prof. Dr. W. Zhu

Key Laboratory for Advanced Materials and Institute of Fine Chemicals, Shanghai Key Laboratory of Functional Materials Chemistry, State Key Laboratory of Bioreactor Engineering, Collaborative Innovation Center for Coal Based Energy (i-CCE), East China University of Science & Technology, Shanghai 200237 (China)

E-mail: whzhu@ecust.edu.cn; guozq@ecust.edu.cn

Dr. J. Guo

PerkinElmer Instruments (Shanghai) Co.

Zhangheng Road 1670 Shanghai 201203 (China)

Prof. Dr. T. James

Department of Chemistry, University of Bath

Bath BA2 7AY, United Kingdom

[+] These authors contributed equally to this work

[**] This work was supported by NSFC for Creative Research Groups (21421004) and Distinguished Young Scholars (21325625), National 973 Program (2013CB733700), NSFC/China, Oriental Scholarship, Shanghai Pujiang Program (13PJD010), Fok Ying Tong Education Foundation (142014), Fundamental Research Funds for the Central Universities (222201313010) and Catalysis and Sensing for our Environment (CASE) network.

Supporting information for this article is available on the WWW under http://www.angewandte.org or from the author.

Abstract: *The rational design of high-performance fluorescent materials for cancer targeting in vivo is still challenging. Here we report the unique molecular design strategy by tailoring aggregation-induced emission (AIE)-active organic molecules to realize preferable far-red and NIR fluorescence, well-controlled morphology from rod-like to spherical, as well as tumor targeted bioimaging. The shape-tailored organic quinoline-malononitrile (QM) nanoprobes are biocompatible, and highly desirable for cell tracking applications. Impressively, the spherical shape of QM-5 nanoaggregates exhibits excellent tumor-targeted bioimaging performance after intravenously injection into mice, but not the rod-like aggregates of QM-2.*

The development of bioimaging probes that can differentiate tumors from normal tissues are highly desirable for cancer diagnosis and therapy *in vivo*.[1,2] Fluorescent materials that provide dynamic and quantitative information of imaging biomolecules have become indispensable tools for biological analysis and clinical diagnosis.[3,4] In particular, organic nanomaterials with excellent synthetic flexibility for chemical modification are advantageous for real-time cell visualizations, diagnosis and treatment of diseases *in vivo*.[5] While nanomaterial bioimaging displays a critical interdependent role of particle shape, size and surface chemistry (such as polymers, liposomes, dendrimers, immunoconjugates, carbon nanotubes, porphysomes and inorganic particles),[6] methods to rationally tailor small molecules to afford organic nanostructures with the desired morphology, and therefore performing ideal function in diagnosis or therapy *in vivo* is less understood.

Several impressive photo-electronic materials with well-defined morphologies can be obtained using tailor-made small molecules,[7] but these functional self-assemble materials remain further exploration on biomedical application, mainly due to several limitations: i) inherent fluorescence quenching which is common for most organic fluorophores during their aggregation in aqueous media; ii) lacking high-performance near-infrared (NIR) emission; and iii) the unclear relationship between tailored morphologies and targeting efficacy for *in vivo* diagnostics. Fortunately, since the concept of aggregation-induced emission (AIE) was originally reported by Tang *et al*,[8a] AIE-active molecules exhibit highly

bright fluorescence when aggregated, and weak fluorescence when separated in solution,[8] making them ideal for biosensing and imaging *in vivo*. However, mapping the nature of AIE-active organic molecules to finely control the morphologies and sizes of organic aggregated nanostructures is uncharted territory, especially the influence of substituents on the shape, and therefore the excellent optical properties for bioimaging *in vivo*.

As well known, far-red and NIR emission could minimize photo-damage to living cells, enable deep tissue penetration, and circumvent the spectral overlap with biosubstrate autofluorescence.[9] While great efforts have been made towards the development of high-performance AIE-active systems for long-term non-invasive bioimaging *in vivo*,[8b] the majority of AIE luminogens has emission wavelengths below 650 nm. Particularly, it is not clear whether AIE nanoaggregates with specific morphologies are suitable for targeted imaging *in vivo*. Herein we set out to construct a tailor-made far-red and NIR AIE-active system (Figure 1A) employing the quinoline-malononitrile (QM) as AIE building block[8f], wherein the morphology of organic nanostructures could be controlled by changing the electron donor groups and thiophene π-bridge. Different shapes of these AIE-active QM derivatives with red to NIR emission were carefully evaluated under an aggregated microenvironment, thus taking insight into the effect of specific shape on both real-time cell tracing and tumor-targeted imaging *in vivo*.

We performed a series of experiments to examine the photoluminescence properties of QM derivatives. As expected, all QM compounds exhibit red to NIR AIE-active characteristics along with an increasing volume fraction of water in tetrahydrofuran/water (THF/H_2O) mixtures (Figure 1, Figure S1 and Table S1 in the Supporting Information). Moreover, their fluorescent properties are dependent upon the aggregated microenvironment. Specifically for QM-1, a strong fluorescence was not observed until the volume fraction of water (f_w) in THF/H_2O solutions up to 80% (Figure 1B). Its fluorescence quantum yield (Φ_F) exhibited AIE light-up enhancement by 178-fold in the mixed f_w = 90% THF/H_2O solution compared with that in pure THF solution.

When strong donor groups are introduced into the thiophene moiety elongating the π-conjugated systems of the QM molecules, their emission spectra are extended to deep red, and even to the NIR region.

As shown in Figure 1C, with a gradual addition of water into THF, QM-2 molecules containing the triphenylamine donor clustered into nanoaggregates and the emission was dramatically enhanced with an f_w increase, showing an obvious AIE effect. Successively, the emission spectra showed a little decrease when f_w > 80%, which might be attributed that QM-2 molecules aggregate and precipitate quickly at higher water fraction, leading to amorphous agglomerates formation with lower fluorescence intensity.[10] Moreover, the fluorescence quantum yield (Φ_F) of QM-2 was increased sharply by about 183-fold from pure THF solution to the mixed THF/H_2O (f_w = 70%) solution. Furthermore, when a stronger alkoxytriphenylamine donor moiety was introduced into QM-3, the emission peak located at 672 nm in pure THF was observed in its molecularly dissolved state. When water was mixed with THF (f_w > 50%), its emission spectra was bathochromically shifted to 705 nm with intensified AIE-active emission.

To further take insight into the substituent influence, a 3,4-ethylene-dioxythiophene (EDOT) unit was introduced into QM-2 to give QM-4, in which the steric hindrance of EDOT can change the initial D-π-A structure into more twist structure. In fact, the structural and conformational differences of QM derivatives are responsible for the different aggregated microenvironment, thus resulting in different AIE-active spectral features. As demonstrated by the X-ray diffraction (XRD) patterns (Figure S2 in SI), QM-4 aggregates are mainly in amorphous state, which might affect its fluorescent quantum yield.[10] Indeed, QM-4 exhibited 17-fold enhancement in Φ_F value from f_w = 0 to 70% in a mixed THF/H_2O solution, and concomitantly the emission peak was red-shifted from 642 to 669 nm (Figure 1D).

Following this line of thought, a combinational molecular strategy was employed in the design of QM-5, wherein the alkoxy-substituted triphenylamine moiety as a stronger donor would extend the NIR emission spectra, and EDOT-substituted thiophene would disrupt the linear D-π-A structure for tailoring the aggregate formation. Similar to QM-4, with an increase in water fraction, the emission spectra of QM-5 exhibited a large red shift from 668 nm in pure THF solution to 721 nm in f_w = 90% of the mixed THF/H_2O solution (Figure 1E). To further verify our molecular design strategy, QM-6 was designed and synthesized, which also endowed similar AIE-active fluorescence properties. As a consequence, we are

able to extend the long wavelength AIE-active luminescence of QM derivatives from 612 to 721 nm in THF/H_2O solution (Figure 1F), and even from 651 to 738 nm in their solid state (Figure 1G).

[Figure 1]

In order to explore the influence of substituents on the nanostructures, we employed a solution evaporation approach to fabricate QM aggregates. Indeed, the progressive transformation of morphology for QM aggregates were successfully observed, characterized with transmission electron microscopy (TEM), scanning electron microscopy (SEM) and confocal laser scanning microscopy (CLSM). As shown in Figure 2A-I, the aggregates of QM-1, QM-2 and QM-3 were well-defined microrods with different sizes and diameters. For instance, the uniform 1-D microrods of QM-2 were observed by SEM with the size of about 10 μm in length and 0.5-1 μm in diameter (Figure 2E). The TEM and CLSM images in Figures 2D and 2F further verified rod-like microstructures in the aggregates of QM-2. Similar morphological characteristics could also be observed in QM-1 and QM-3 aggregates, demonstrating strong AIE-active fluorescence and easily linear self-aggregation when thiophene was utilized as a π-conjugated bridge in the QM derivatives. Fortunately, the single crystals of QM-1, QM-2 and QM-3 were obtained by the slow evaporation approach (Table S2 and Figure S3 in SI). All QM-1, QM-2 and QM-3 display twisted conformations in their crystal structures with large torsional angles of 85.4~87.0º between the *N*-ethyl and the quinoline units (Figure 1A). In addition, moderate interplanar angles of 32.2~35.3º are observed between the ethylene and quinoline units, and no obvious π-π stacking interactions can be found in the crystals, which may be ascribed to the twisted molecular structures. As a result, their aggregation states display enhanced emission.

However, for QM-4, QM-5 and QM-6 (Figure 2J-R), instead of the microrod structures, the resulting morphology was predominated with spherical shaped nanoparticles in diameter of about 80-200 nm. This might be ascribed to the attachment of an epoxyethyl group in the EDOT π-bridge, leading to a totally different intermolecular interaction in the aggregation state. Moreover, the average diameters of QM-5

aggregates measured by laser light scattering (LLS) were about 85 (±10) nm, exactly in consistent with the data from SEM images (90±10 nm). Under the same fabricating conditions, the TEM images of QM-5 had the smallest diameters and smoothest spherical morphologies with respect to QM-4 and QM-6 (Figure S4 in SI).

Based on the rational molecular design, the flexibility and electron rich properties of the epoxy ethyl groups in QM chemical structures play important roles in the morphological formation during the aggregation process when EDOT is introduced as the π-conjugated bridge. It is expected that the incorporation of both alkoxytriphenylamine group and EDOT unit in QM derivatives is a preferable design strategy to generate AIE-active spherical nanostructures, resulting in a distinct change in morphology from QM-1 to QM-6 (Figure 2).

[Figure 2]

Considering nanoprobes for bioimaging *in vivo*, it is necessary to assess the external influence on aggregation and photostability of AIE materials. As shown in Figure S5-6 in SI, once QM derivatives have formed into aggregation state under the optimized f_w, external factors have little effect on the morphology of QM aggregates. Also the photostability of AIE-active QM materials and commercial ICG dye (approved by FDA for NIR clinical imaging agents) was evaluated by time-course fluorescence measurement. After exposure to high density light, the half-life time of QM derivatives was about 20-fold longer than ICG dye, demonstrating that QM derivatives are more photostable materials.

Among all the QM derivatives, QM-2 and QM-5 are the typical representatives of rod-like and spherical shapes, respectively. Thus, we chose these two compounds to further explore their potential shape effects on *in vitro* and *in vivo* applications in living system. Exactly, QM-2 and QM-5 exhibited low toxicity against both cancer cells and normal cells, highly preferable for cell imaging or tracking applications (Figures S7-S10 in SI). Flow cytometric studies were conducted to evaluate the kinetics of the cell uptake process of QM-2 and QM-5 in the Hela cells. Although the relative uptake ratio of both

compounds after 48 h incubation was close to 100% (≥ 99.5%), the initial uptake rate of QM-5 was much faster compared to that of QM-2. Additionally, the CLSM images presented a direct observation of the spherical shape of QM-5 in cells.

The high-brightness emission for AIE-active organic nanomaterials could be used as efficient long-term cell tracers. For instance, QM-2, QM-5 and commercial ICG dye as control showed bright fluorescence after incubation with Hela cells for 24 h in spite of the different retention in the cytoplasm of Hela cells (with the potential as long-term cell tracers). For QM-2 and QM-5, even after four passages of incubation with living cells, the fluorescence of QM aggregates staining in Hela cells was still emissive. In contrast, there was almost no fluorescence signal using ICG at two passages of incubation. Therefore, the formation of high biocompatible and photostable AIE-active QM aggregates with different shape and size is beneficial to retain fluorescence in the cells, desirable for long term cell tracing.

The promising long-term cell tracing results of AIE-active QM derivatives inspired us to further explore their feasibility as NIR bioprobes *in vivo*. Upon intravenous injection of QM-2 at a dose of 0.15 mg/kg, we immediately monitored the fluorescence distribution in mice at different periods of time. As shown in Figure 3A, the fluorescence was clearly observed in mice at 30 min, indicative of the rapid distribution of QM-2 aggregates via the blood circulation. Surprisingly, upon the paralleled intravenous injection of QM-5 (0.15 mg/kg, Figure 3B), the distinct NIR fluorescence could predominately be detected in the tumor at 30 min, rather than other organs of the mouse, and retained in tumor tissue even at 24 h after injection. The long retention of the QM-5 nanoaggreates in tumors makes this system very promising for tumor labeling and chemotherapy. However, even at 24 h after the injection, the QM-2 aggregates were still present in the whole mouse body biodistribution without producing tumor-targeted fluorescence signals *in vivo.* Similar phenomenon was also observed for another rod-like nanostructure QM-3 (Figure S11 in SI), further confirming the non-specific *in vivo* imaging biodistribution of organic rod-like QM assemblies.

The *ex vivo* fluorescence images of the internal organs of mice sacrificed at 24 h post-injection in Figure 3D also indicated that QM-5 aggregates accumulated in the tumor and liver tissue, whereas the

fluorescence of QM-2 aggregates in tumor was much weaker than other organs such as liver or lung (Figure 3C). Furthermore, the 3D fluorescence imaging of tumor-bearing mice in Figure 3E at 24 h post-injection of QM-5 (0.15 mg/kg) further confirmed the NIR fluorescence accumulation in tumors. Accordingly, the semi-quantitative analysis data of the average fluorescence intensity distribution in organs (Figure 3F) also demonstrated that the spherical shape of QM-5 aggregates exhibited much higher tumor-targeting ability than the rod-like aggregates of QM-2.

Undoubtedly, in contrast with the fast degradation in aqueous media and quick clearance from the body of small molecular imaging agent ICG dye[11] (control, Figure S12 in SI), the shape-specificity of QM aggregates contributes a direct benefit for long-term retention and bioimaging *in vivo*. Actually, from the TEM images of cells and tissues, we clearly observed that QM aggregates almost maintained their initial aggregated morphologies *in situ* (Figure S13 in SI). While the fluorescence of rod-like aggregates by QM-2 exhibited the whole body biodistribution in mice, the spherical QM-5 aggregates enhanced tumor-targeting capacity, which could be ascribed to the "passive" tumor-targeting by enhanced permeability and retention (EPR) effect.[12] Apparently, here the particle geometry plays an important role in the tumor-targeted bioimaging *in vivo*. Another potential possibility for this disparity could be the difference in shape and shape-related factors such as curvature and aspect ratio, which affect cell-particle interactions, particle transport characteristics and margination dynamics.[6k,12] Therefore, based on the TEM images of Hela cells and tissues, the shape differences of QM aggregates formed by tailoring AIE-active organic molecules are of great value for tumor-targeted bioimaging *in vivo*.

[Figure 3]

In summary, far-red and NIR AIE-active fluorescent organic QM nanoprobes have been rationally designed. We specifically focused on the modulation of long emitting wavelength and the aggregated morphologies *via* essentially tailoring π-bridge and donor unit in molecular structures. QM derivatives from rod-like to spherical morphology were well confirmed by SEM, TEM and CLSM images. *In vitro*

experiments have verified that these tailor-made long wavelength AIE-active organic QM nanomaterials are biocompatible and retained in the cytoplasm of living cells. The most striking feature of NIR spherical QM-5 nanoaggregates is their excellent tumor-targeting performance in mice. Conversely, the same is not true for the rod-like aggregates of QM-2 which does not display any tumor targeting properties. To the best of our knowledge, this is the first report of shape-specific tumor targeting using bare NIR AIE-active nanoprobes. Our strategy generates high-performance long wavelength AIE-active organic nanomaterials with ideal biological geometries for tumor-targeted bioimaging *in vivo*, providing a promising platform for *in situ* and *in vivo* tumor imaging agents.

Received: ((will be filled in by the editorial staff))

Published online on ((will be filled in by the editorial staff))

Keywords: Far-red and NIR, Aggregation-induced emission, Fluorescent probe, Morphology, Tumor targeting

[1] a) P. D. Howes, R. Chandrawati, M. M. Stevens, *Science* **2014**, *346*, 53; b) M. P. Melancon, M. Zhou, C. Li, *Acc. Chem. Res.* **2011**, *44*, 947-956; c) X. Q. Chen, T. Pradhan, F. Wang, J. S. Kim, J. Yoon, *Chem. Rev.* **2012**, *112*, 1910-1956; d) V. Shanmugam, S. Selvakumar, C.-S. Yeh, *Chem. Soc. Rev.* **2014**, *43*, 6254-6287; e) Q. L. Fan, K. Cheng, X. Hu, X. W. Ma, R. P. Zhang, M. Yang, X. M. Lu, L. Xing, W. Huang, S. S. Gambhir, Z. Cheng, *J. Am. Chem. Soc.* **2014**, *136*, 15185-15194.

[2] a) S. Chapman, M. Dobrovolskaia, K. Farahani, A. Goodwin, A. Joshi, H. Lee, T. Meade, M. Pomper, K. Ptak, J. H. Rao, R. Singh, S. Sridhar, S. Stern, A. Wang, J. B. Weaver, G. Woloschak, L. Yang, *Nano Today* **2013**, *8*, 454-460; b) S. G. Hou, L. Liang, S. H. Deng, J. F. Chen, Q. Huang, Y. Cheng, C. H. Fan, *Sci. China Chem.* **2014**, *57*, 100-106.

[3] a) J. Yao, M. Yang, Y. X. Duan, *Chem. Rev.* **2014**, *114*, 6130-6178; b) E. M. Nolan, S. J. Lippard, *Acc. Chem. Res.* **2009**, *42*, 193-203; c) T. Myochin, K. Hanaoka, T. Komatsu, T. Terai, T. Nagano, *J. Am. Chem. Soc.* **2012**, *134*, 13730-13737; d) M. Schäferling, *Angew. Chem.* **2012**, *124*, 3590-3614;

Angew. Chem. Int. Ed. **2012**, *51*, 3532-3554; e) J. Chan, S. C. Dodani, C. J. Chang, *Nat. Chem.* **2012**, *4*, 973-984; f) Z. Q. Guo, S. Park, J. Yoon, I. Shin, *Chem. Soc. Rev.* **2014**, *43*, 16-29; g) Q. L. Hu, M. Gao, G. X. Feng, B. Liu, *Angew. Chem.* **2014**, *126*, 14449-14453; *Angew. Chem. Int. Ed.* **2014**, *53*, 14225-14229; (h) X. Wu, Z. Li, X.-X. Chen, J. S. Fossey, T. D. James, Y.-B. Jiang, *Chem. Soc. Rev.* **2013**, *42*, 8032-8048.

[4] a) M. H. Lee, N. Park, C. Yi, J. H. Han, J. H. Hong, K. P. Kim, D. H. Kang, J. L. Sessler, C. Kang, J. S. Kim, *J. Am. Chem. Soc.* **2014**, *136*, 14136-14142; b) X. J. Peng, T. Wu, J. L. Fan, J. Y. Wang, S. Zhang, F. L. Song, S. G. Sun, *Angew. Chem.* **2011**, *123*, 4266-4269; *Angew. Chem. Int. Ed.* **2011**, *50*, 4180-4183; c) W. M. Xuan, C. Q. Sheng, Y. T. Cao, W. H. He, W. Wang, *Angew. Chem.* **2012**, *124*, 2328-2330; *Angew. Chem. Int. Ed.* **2012**, *51*, 2282-2284; d) T. Yoshii, K. Mizusawa, Y. Takaoka, I. Hamachi, *J. Am. Chem. Soc.* **2014**, *136*, 16635-16642; e) G. Ghale, W. M. Nau, *Acc. Chem. Res.* **2014**, *47*, 2150-2159; (f) V. Kumar, E. V. Anslyn, *J. Am. Chem. Soc.* **2013**, *135*, 6338-6344; (g) J. Y. Shao, H. Y. Sun, H. M. Guo, S. M. Ji, J. Z. Zhao, W. T. Wu, X. L. Yuan, C. L. Zhang, T. D. James, *Chem. Sci.* **2012**, *3*, 1049-1061.

[5] a) X. L. Hu, J. M. Hu, J. Tian, Z. S. Ge, G. Y. Zhang, K. F. Luo, S. Y. Liu, *J. Am. Chem. Soc.* **2013**, *135*, 17617-17629; b) D. Ding, K. Li, B. Liu, B. Z. Tang, *Acc. Chem. Res.* **2013**, *46*, 2441-2453; c) X. M. Wu, W. H. Zhu, *Chem. Soc. Rev.* **2015**, doi:10.1039/c4cs00152d; d) P. Anees, S. Sreejith, A. Ajayaghosh, *J. Am. Chem. Soc.* **2014**, *136*, 13233-13239.

[6] a) S. Barua, J.-W. Yoo, P. Kolhar, A. Wakankar, Y. R. Gokarn, S. Mitragotri, *Proc. Natl. Acad. Sci. U.S.A.* **2013**, *110*, 3270-3275; b) L. K. Truman, S. Comby, T. Gunnlaugsson, *Angew. Chem.* **2012**, *124*, 9762-9765; *Angew. Chem. Int. Ed.* **2012**, *51*, 9624-9627; c) X. R. Duan, L. B. Liu, F. D. Feng, S. Wang, *Acc. Chem. Res.* **2010**, *43*, 260-270; d) Z. L. Zhao, H. M. Meng, N. N. Wang, M. J. Donovan, T. Fu, M. X. You, Z. Chen, X. B. Zhang, W. H. Tan, *Angew. Chem.* **2013**, *125*, 7635-7639; *Angew. Chem. Int. Ed.* **2013**, *52*, 7487-7491; e) L. Tao, W. Hu, Y. L. Liu, G. Huang, B. D. Sumer, J. M. Gao, *Exp. Biol. Med.* **2011**, *236*, 20-29; f) P. Decuzzi, B. Godin, T. Tanaka, S.-Y. Lee, C. Chiappini, X. Liu, M. Ferrari, *J. Controlled Release* **2010**, *141*, 320-327; g) S. E. A. Gratton, P. A. Ropp, P. D.

Pohlhaus, J. C. Luft, V. J. Madden, M. E. Napier, J. M. Desimone, *Proc. Natl. Acad. Sci. U.S.A.* **2008**, *105*, 11613-11618; h) Y. Geng, P. Dalhaimer, S. S. Cai, R. Tsai, M. Tewari, T. Minko, D. E. Discher, *Nat. Nanotechnol.* **2007**, *2*, 249-255; i) J. F. Lovell, C. S. Jin, E. Huynh, H. Jin, C. Kim, J. L. Rubinstein, W. C. W. Chan, W. Cao, L. V. Wang, G. Zheng, *Nat. Mater.* **2011**, *10*, 324-332; j) K. K. Ng, J. F. Lovell, A. Vedadi, T. Hajian, G. Zheng, *ACS Nano* **2013**, *7*, 3484-3490; k) B. D. Chithrani, W. C. W. Chan, *Nano Lett.* **2007**, *7*, 1542-1550.

[7] a) Z. Y. Tian, Y. Chen, W. S. Yang, J. N. Yao, L. Y. Zhu, Z. G. Shuai, *Angew. Chem.* **2004**, *116*, 4152-4155; *Angew. Chem. Int. Ed.* **2004**, *43*, 4060-4063; b) R. Yoshii, A. Hirose, K. Tanaka, Y. Chujo, *J. Am. Chem. Soc.* **2015**, *136*, 18131-18139; c) Y. L. Yan, Y. S. Zhao, *Chem. Soc. Rev.* **2014**, *43*, 4325-4340; d) W. Yao, Y. L. Yan, L. Xue, C. Zhang, G. P. Li, Q. D. Zheng, Y. S. Zhao, H. Jiang, J. N. Yao, *Angew. Chem.* **2013**, *125*, 8875-8879; *Angew. Chem. Int. Ed.* **2013**, *52*, 8713-8717; e) W. Wang, L. Q. Wang, B. J. Palmer, G. J. Exarhos, A. D. Q. Li, *J. Am. Chem. Soc.* **2006**, *128*, 11150-11159.

[8] a) J. D. Luo, Z. L. Xie, J. W. Y. Lam, L. Cheng, H. Y. Chen, C. F. Qiu, H. S. Kwok, X. W. Zhan, Y. Q. Liu, D. B. Zhu, B. Z. Tang, *Chem. Commun.* **2001**, 1740-1741; b) R. T. K. Kwok, C. W. T. Leung, J. W. Y. Lam, B. Z. Tang, *Chem. Soc. Rev.* **2015**, DOI: 10.1039/c4cs00325j; c) Y. Y. Yuan, C.-J. Zhang, M. Gao, R. Y. Zhang, B. Z. Tang, B. Liu, *Angew. Chem.* **2015**, *127*, 1800-1806; *Angew. Chem. Int. Ed.* **2015**, *54*, 1780-1786; d) B.-K. An, S.-K. Kwon, S.-D. Jung, S. Y. Park, *J. Am. Chem. Soc*. **2002**, *124*, 14410-14415; e) L. Yao, S. T. Zhang, R. Wang, W. J. Li, F. Z. Shen, B. Yang, Y. G. Ma, *Angew. Chem.* **2014**, *126*, 2151-2155; *Angew. Chem. Int. Ed.* **2014**, *53*, 2119-2123; f) C. X. Shi, Z. Q. Guo, Y. L. Yan, S. Q. Zhu, Y. S. Xie, Y. S. Zhao, W. H. Zhu, H. Tian, *ACS Appl. Mater. Interfaces* **2013**, *5*, 192-198; g) A. D. Shao, Z. Q. Guo, S. J. Zhu, S. Q. Zhu, P. Shi, H. Tian, W. H. Zhu, *Chem. Sci.* **2014**, *5*, 1383-1389; h) F. Hu, Y. Y. Huang, G. X. Zhang, R. Zhao, H. Yang, D. Q. Zhang, *Anal. Chem.* **2014**, *86*, 7987-7995; i) X. Q. Zhang, X. Y. Zhang, B. Yang, Y. L. Zhang, Y. Wei, *ACS Appl. Mater. Interfaces* **2014**, *6*, 3600-3606; j) D. D. Li, C. L. Miao, X. D. Wang, X. H. Yu, J. H. Yu, R. R. Xu, *Chem. Commun.* **2013**, 49, 9549-9551; k) S. Pramanik, V. Bhalla, M. Kumar,

ACS Appl. Mater. Interfaces **2014**, *6*, 5930-5939; (l) S. D. Xu, T. T. Liu, Y. X. Mu, Y. F. Wang, Z. G. Chi, C.-C. Lo, S. W. Liu, Y. Zhang, A. Lien, J. R. Xu, *Angew. Chem.* **2015**, *127*, 888-892; *Angew. Chem. Int. Ed.* **2015**, *54*, 874 –878.

[9] a) R. Weissleder, M. J. Pittet, *Nature* **2008**, *452*, 580-589; b) Y. Liu, M. Chen, T. Y. Cao, Y. Sun, C. Y. Li, Q. Liu, T. S. Yang, L. M. Yao, W. Feng, F. Y. Li, *J. Am. Chem. Soc.* **2013**, *135*, 9869-9876; c) X. M. Wu, X. R. Sun, Z. Q. Guo, J. B. Tang, Y. Q. Shen, T. D. James, H. Tian, W. H. Zhu, *J. Am. Chem. Soc.* **2014**, *136*, 3579-3588; d) A. Atilgan, E. T. Ecik, R. Guliyev, T. B. Uyar, S. Erbas-Cakmak, E. U. Akkaya, *Angew. Chem.* **2014**, *126*, 10854-10857; *Angew. Chem. Int. Ed.* **2014**, *53*, 10678-10681.

[10] a) X. Y. Shen, Y. J. Wang, E. G. Zhao, W. Z. Yuan, Y. Liu, P. Lu, A. J. Qin, Y. G. Ma, J. Z. Sun, B. Z. Tang, *J. Phys. Chem. C* **2013**, *117*, 7334-7347; b) H. Tong, Y. N. Hong, Y. Q. Dong, Y. Ren, M. Häussler, J. W. Y. Lam, K. S. Wong, B. Z. Tang, *J. Phys. Chem. B* **2007**, *111*, 2000-2007.

[11] K. Miki, Y. Kuramochi, K. Oride, S. Inoue, H. Harada, M. Hiraoka, K. Ohe, *Bioconjugate Chem.* **2009**, *20*, 511-517.

[12] a) H. Maeda, J. Wu, T. Sawa, Y. Matsumura, K. Hori, *J. Controlled Release* **2000**, *65*, 271-284; b) T. M. Allen, P. R. Cullis, *Science* **2004**, *303*, 1818-1822; c) M. Caldorera-Moore, N. Guimard, K. Roy, *Expert. Opin. Drug Deliv*. **2010**, 7, 479-495.

Legends for Figures and Schemes and Tables

Figure 1. QM derivatives and AIE properties: (A) Molecular structures and the single crystal configurations of QM-1, QM-2 and QM-3. Photoluminescence spectra and plot of the relative PL intensity of QM derivatives (10^{-5} M): (B) QM-1, (C) QM-2, (D) QM-4 and (E) QM-5 in THF/H_2O mixtures with different volume fractions of water (f_w); λ_{ex} = 480 nm. Inset: Fluorescent photoimages in pure THF solvent and THF/H_2O solution of (B) QM-1 (f_w = 90%), (C) QM-2 (f_w = 70%), (D) QM-4 (f_w = 70%) and (E) QM-5 (f_w = 90%) under 365 nm illumination. (F) Normalized fluorescent spectra of QM-1 (f_w = 90%), QM-2 (f_w = 70%), QM-3 (f_w = 90%), QM-4 (f_w = 70%), QM-5 (f_w = 90%) and QM-6 (f_w = 90%) in THF/H_2O solution. (G) Normalized fluorescent spectra of QM derivatives in the solid state.

Figure 2. Multiple morphologies of micro/nanoaggregates fabricated from QM derivatives (10^{-5} M). TEM, SEM and confocal laser scanning microscope (CLSM) images recorded for the micro/nanoaggregates of QM-1 (A-C), QM-2 (D-F), QM-3 (G-I), QM-4 (J-L), QM-5 (M-O) and QM-6 (P-R), prepared by adding different content of water into pure THF solution to afford the mixed solution of THF/H_2O then still standing for 1 h.

Figure 3. *In vivo* non-invasive imaging of tumor-bearing mice after intravenous injection of (A) QM-2 (0.15 mg/kg), (B) QM-5 (0.15 mg/kg) at different periods of time (0.5, 1.5, 3 and 24 h), and *ex vivo* fluorescence images of the internal organs of mice sacrificed at 24 h post-injection with (C) QM-2 and (D) QM-5. (E) The 3D fluorescence imaging of tumor-bearing mice after intravenous injection of QM-5 (0.15 mg/kg) for 24 h. (F) Average fluorescence intensity distribution for tumor and internal organs from mice sacrificed at 24 h post-injection with QM-2 and QM-5 (n = 3).

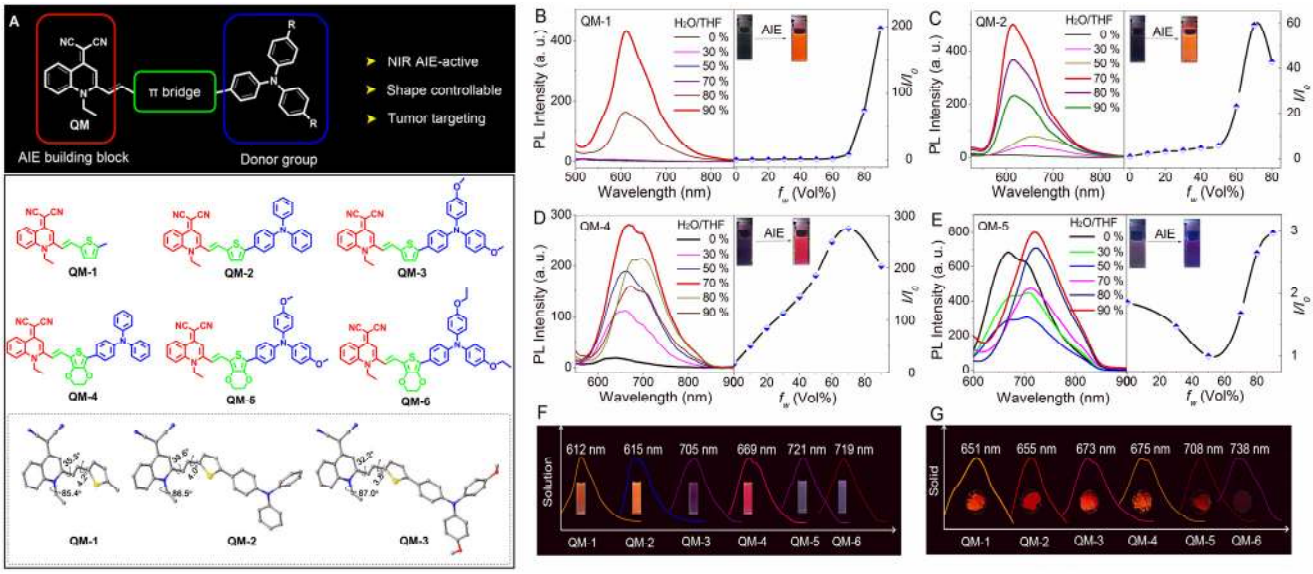

Figure 1. QM derivatives and AIE properties: (A) Molecular structures and the single crystal configurations of QM-1, QM-2 and QM-3. Photoluminescence spectra and plot of the relative PL intensity of QM derivatives (10^{-5} M): (B) QM-1, (C) QM-2, (D) QM-4 and (E) QM-5 in THF/H_2O mixtures with different volume fractions of water (f_w); λ_{ex} = 480 nm. Inset: Fluorescent photoimages in pure THF solvent and THF/H_2O solution of (B) QM-1 (f_w = 90%), (C) QM-2 (f_w = 70%), (D) QM-4 (f_w = 70%) and (E) QM-5 (f_w = 90%) under 365 nm illumination. (F) Normalized fluorescent spectra of QM-1 (f_w = 90%), QM-2 (f_w = 70%), QM-3 (f_w = 90%), QM-4 (f_w = 70%), QM-5 (f_w = 90%) and QM-6 (f_w = 90%) in THF/H_2O solution. (G) Normalized fluorescent spectra of QM derivatives in the solid state.

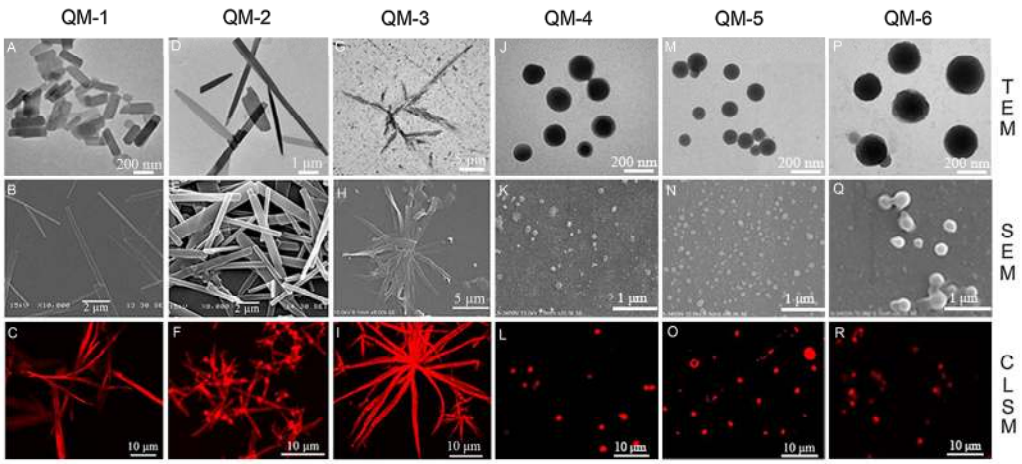

Figure 2. Multiple morphologies of micro/nanoaggregates fabricated from QM derivatives (10^{-5} M). TEM, SEM and confocal laser scanning microscope (CLSM) images recorded for the micro/nanoaggregates of QM-1 (A-C), QM-2 (D-F), QM-3 (G-I), QM-4 (J-L), QM-5 (M-O) and QM-6 (P-R), prepared by adding different content of water into pure THF solution to afford the mixed solution of THF/H_2O then still standing for 1 h.

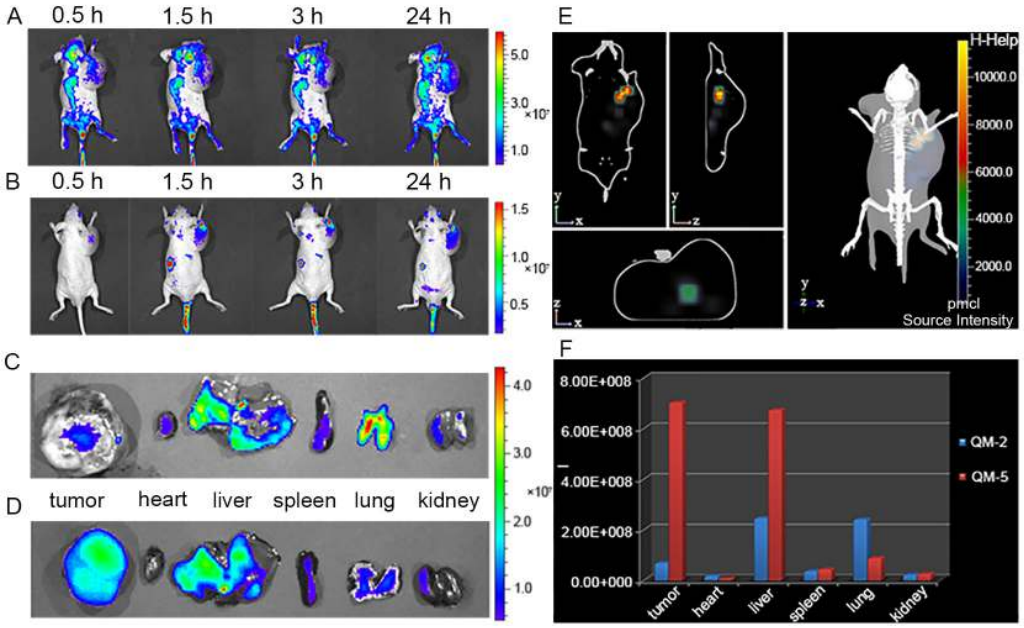

Figure 3. *In vivo* non-invasive imaging of tumor-bearing mice after intravenous injection of (A) QM-2 (0.15 mg/kg), (B) QM-5 (0.15 mg/kg) at different periods of time (0.5, 1.5, 3 and 24 h), and *ex vivo* fluorescence images of the internal organs of mice sacrificed at 24 h post-injection with (C) QM-2 and (D) QM-5. (E) The 3D fluorescence imaging of tumor-bearing mice after intravenous injection of QM-5 (0.15 mg/kg) for 24 h. (F) Average fluorescence intensity distribution for tumor and internal organs from mice sacrificed at 24 h post-injection with QM-2 and QM-5 (n=3).